Editors' Suggestion

Experimental Quantum Key Distribution with Integrated Silicon Photonics and Electronics

Chen-Xi Zhu,[1] Zhao-Yuan Chen,[2,3,4,5] Yang Li,[2,3,4,*] Xin-Zhe Wang,[2,3,4,†] Chao-Ze Wang,[1,2,3,4] Yu-Long Zhu,[6] Fu-Tian Liang,[2,3,4] Wen-Qi Cai,[2,3,4] Ge Jin,[6] Sheng-Kai Liao,[1,2,3,4,‡] and Cheng-Zhi Peng[2,3,4]

[1] *School of Cyberspace Security, University of Science and Technology of China, Hefei 230026, China*
[2] *Hefei National Research Center for Physical Sciences at the Microscale and School of Physical Sciences, University of Science and Technology of China, Hefei 230026, China*
[3] *Shanghai Research Center for Quantum Science and CAS Center for Excellence in Quantum Information and Quantum Physics, University of Science and Technology of China, Shanghai 201315, China*
[4] *Hefei National Laboratory, University of Science and Technology of China, Hefei 230088, China*
[5] *PLA Rocket Force University of Engineering, Xi'an 710025, China*
[6] *Department of Modern Physics, University of Science and Technology of China, Hefei 230026, China*

(Received 5 January 2022; accepted 12 May 2022; published 16 June 2022)

Quantum key distribution (QKD) provides a methodology for secure key distribution based on fundamental physical laws. Although significant experimental progress has been made, the previous QKD systems are mainly composed of discrete optical and electronic devices. Here, we present a prototype of a QKD transmitter by developing the technologies of integrated silicon photonics and electronics. The photonic chip integrates the essential encoding components for the decoy-state BB84 protocol using polarization encoding, while the electronic chips integrate the dedicated driving circuits. On the basis of these integrated chips, we build a desktop QKD system to verify their performance. Successful QKD experiments are conducted at a repetition frequency of 312.5 MHz using standard fiber and emulated channel loss and the intrinsic quantum bit error rate of the system is as low as 0.41%. The finite-key secret rate is 42.7 kbit/s for the 100-km fiber and 295.5 bit/s for the 40-dB emulated loss. Our results demonstrate the feasibility of QKD based on integrated optoelectronic devices and hopefully take a fundamental toward a system-in-a-package solution.

DOI: 10.1103/PhysRevApplied.17.064034

I. INTRODUCTION

Quantum key distribution (QKD) offers a methodology for secure key distribution based on the laws of physics. Since the BB84 QKD protocol was proposed in 1984 [1], it has made significant progress in both fiber link [2–8] and terrestrial free-space link [9–14] optical communications. On the basis of the *Micius* satellite launched in 2016, satellite-to-ground QKD [15–17], a satellite-relayed intercontinental quantum network [18], and an integrated space-to-ground quantum communication network [19] have been already established. Meanwhile, several fiber quantum networks [20–26] have been presented in metropolitan areas for long-term applications. In working toward secure QKD with realistic devices, great efforts have been devoted to studying the deviations of realistic devices from the idealized model and solving them [27–29] or adopting different protocols to close some critical side channels [30–33]. All of these results indicate that QKD has gradually moved from the laboratory to practical applications.

Despite the significant experimental progress that has been made, the previous QKD systems are mainly composed of discrete optical and electronic devices [8,11,12,14]. For example, for the decoy-state-based polarization-encoding BB84 protocol, the polarization encoding and intensity modulation are generally realized by commercial phase modulators together with additional optical modules [5,14] such as the Mach–Zehnder-interferometer [5,6] or Sagnac-interferometer structure [34,35]. In order to drive the laser diode (LD) and phase modulators, specific electronic devices are essential. In previous QKD demonstrations, electronic driving devices have been realized either by using bulky general-purpose instruments [36] or by developing complex dedicated drive circuits [12]. In working toward a global quantum network with

*liyang9@ustc.edu.cn
†wxzyf@ustc.edu.cn
‡skliao@ustc.edu.cn

 © 2022 American Physical Society

practical applications, QKD systems consisting of discrete optical and electronic devices are not enough to provide a miniaturized low-cost QKD-system solution.

Although integrated photonics has a history of decades of development [37], its application in QKD has just begun. A silicon photonics QKD transmitter has been reported in 2016 [38]. Since that time, plenty of photonics integrated chips (PICs) have been designed to realize different QKD protocols, such as BB84 [39–41], coherent one-way (COW) [39,42], measurement-device-independent (MDI) [43,44], and continuous-variable (CV) [45] QKD. In addition to Si photonics, integrated photonics based on platforms such as InP [40] and lithium niobate [46] have also acquired some applications. On the basis of these integrated photonics, successful QKD demonstrations have also been conducted in indoor fiber spools [39,43] in a metropolitan area [47] and in a field free-space channel [48] to verify their applicability and performance in practical QKD applications. For electronic modules, up to now, the integrated electronics in QKD applications has mainly been focused on the driving chip of LDs, modulators, and detectors and several pioneering works have been reported. For example, in 2001, Ransijn *et al.* designed a 10-Gbit/s laser and/or modulator driver using a 0.25-μm GaAs pseudomorphic high-electron-mobility transistor (pHEMT) process [49]. In 2011, Knochenhauer *et al.* designed a 40-Gbit/s modulation driver using a 0.25-μm Si-Ge bipolar complementary metal oxide semiconductor (BiCMOS) process and an improved breakdown voltage multiplier structure [50]. In 2020, Wang *et al.* designed a predriver chip using a 130-nm CMOS process [51] that can generate the multiamplitude driving pulses for the electro-optic modulator. In 2021, Wei *et al.* designed an active quench and reset circuit for a single-photon avalanche diode (SPAD) using a 65-nm CMOS technology [52].

Heterogeneous integration and co-packaging of integrated photonics and electronics is the ultimate solution for the next generation of a system on a chip or a system in a package [53]. Numerous attempts have been reported both in the field of optical communication [53,54] and of quantum communication [55–57]. For example, in 2021, Bruynsteen *et al.* designed an integrated balanced homodyne photonic electronic detector [56], which can support shot-noise-limited measurements beyond 20 GHz and has potential application in CV QKD. Also in 2021, Beutel *et al.* designed a detector-integrated on-chip QKD receiver and conducted a successful QKD demonstration yielding secret-key rates of 2.5 Mbit/s for low channel attenuations of 2.5 dB [57]. However, all these works toward system-in-a-package QKD are concentrated on QKD receivers and there have been few works on the QKD transmitter thus far.

In this work, by developing technologies of integrated silicon photonics and electronics, we present the prototype of an integrated optoelectronic QKD transmitter and demonstrate successful QKD experiments at a repetition frequency of 312.5 MHz. On the basis of the integrated silicon photonics and electronics, we realize an intrinsic quantum bit error rate (QBER) of 0.41% and a finite-key secret rate of 42.7 kbit/s for the 100-km fiber and 295.5 bit/s for the 40-dB emulated loss. Our results demonstrate the feasibility of a QKD transmitter based on integrated optoelectronic devices, thus hopefully taking a fundamental step toward the future system-in-a-package QKD solution.

The paper is organized as follows. In Sec. II, the design and structure of the integrated silicon photonic chip and electronic chips are proposed. In Sec. III, a schematic of the QKD experimental setup is given, including detailed introductions to the QKD transmitter and the QKD receiver. In Sec. IV, the QKD experimental results are presented and analyzed. Finally, in Sec. V, we conclude the paper and discuss the perspective of possible future work.

II. INTEGRATED SILICON PHOTONICS AND ELECTRONICS

A. Integrated photonics

The structure of the PIC, which is manufactured by a commercial silicon photonics foundry based on a 180-nm silicon-on-insulator (SOI) process, is shown in Fig. 1(a). All essential encoding components for the decoy-state BB84 protocol are integrated within a footprint of 3×4.8 mm^2. The grating coupler (GC) is used to couple the incident light from the input fiber to the chip waveguide. The two multimode interferometers (MMIs), together with the thermo-optic modulator (TOM) and the carrier-depletion modulator (CDM), form a Mach-Zehnder interferometer (MZI) to realize the intensity modulation for the decoy-state theory. The TOM operates on the principle of the thermo-optic effect of silicon to modulate the phase of the incident light. Since the bandwidth is limited to approximately the kilohertz range, it is used to provide the static bias. The CDM has a modulation bandwidth up to tens of gigahertz based on the plasma-dispersion effect; thus it can applied to realize high-speed modulation. The following two MMIs and the two-dimensional grating coupler (2DGC), together with the CDMs inside, form a polarization modulator that can produce any polarization state. However, noting that only four polarization states of two mutually unbiased bases are required for the BB84 protocol, the additional CDM in the polarization modulator is simplified compared to the intensity modulator. The first CDM of PM1 is used to balance the incident light to the two arms of PM2. The second CDM of PM2 helps to introduce various phase differences (0, $\pi/2$, π, and $3\pi/2$) between the two light components. The two light components are superposed after the 2DGC; thus the four polarization states for the BB84 protocol ($|D\rangle = 1/\sqrt{2}(|H\rangle + |V\rangle)$, $|A\rangle = 1/\sqrt{2}(|H\rangle - |V\rangle)$, $|L\rangle =$

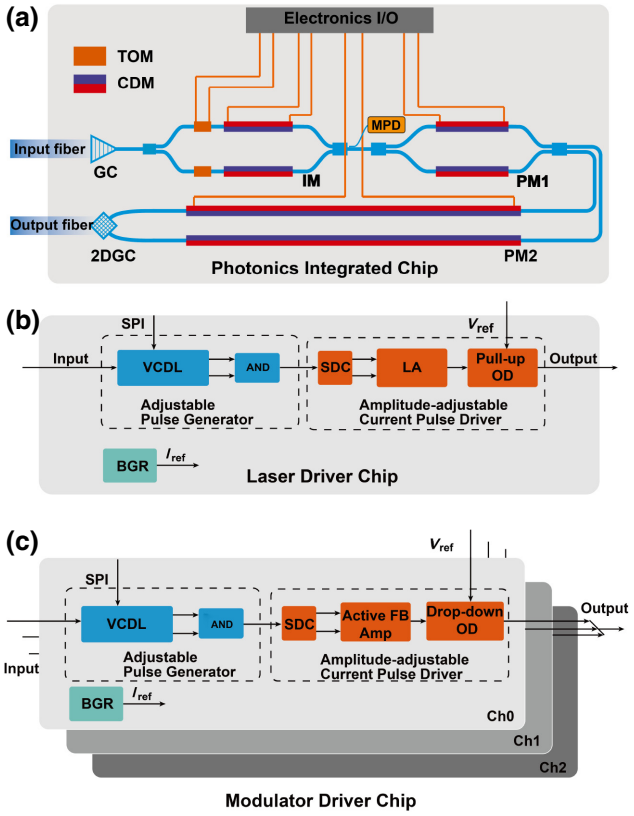


FIG. 1. The structural illustration of the integrated photonic chip and the two integrated electronic chips. (a) A schematic of the photonics integrated chip. All essential encoding components are integrated within a footprint of 3×4.8 mm^2, including a grating coupler (GC) and a two-dimensional grating coupler (2DGC) for the optical input and output, a thermo-optic modulator (TOM) and a carrier-depletion modulator (CDM) as the intensity modulator (IM) and polarization modulator (PM), and a monitor photon detector (MPD) as the optical power monitor. (b) A schematic of the laser driver chip (LDC), which is integrated within a footprint of 1.93×1.2 mm^2. (c) A schematic of the modulator driver chip (MDC), which is integrated within a footprint of 1.44×1.03 mm^2. VCDL, voltage control delay link; SPI, serial peripheral interface; AND, AND gate; SDC, single-ended differential conversion; LA, limiting amplifier; OD, open drain; BGR, band-gap reference; FB, feedback.

$1/\sqrt{2}(|H\rangle + i|V\rangle)$, and $|R\rangle = 1/\sqrt{2}(|H\rangle - i|V\rangle)$) can be prepared.

B. Integrated electronics

The structure of the self-designed laser driver chip (LDC), which is fabricated based on a 130-nm CMOS process, is illustrated in Fig. 1(b) [58]. The LDC mainly includes a pulse generator with adjustable width, a single-ended differential-conversion (SDC) module, a multistage limiting amplifier (LA), and a pull-up open-drain (OD) output stage. The pulse generator receives the input triggering signals and can generate narrow electrical pulses with a specific pulse width based on the low-speed serial peripheral interface (SPI). After the SDC module for single-ended-to-differential conversion, the LA is adopted to amplify the output pulses step by step to ensure the driving ability and signal integrity. The pull-up OD is the output-level module, which can generate a current pulse with an adjustable amplitude based on an external analog voltage (V_{ref}). The band-gap reference (BGR) module provides the reference current for the whole chip. Noting that the LD generally works in the gain-switching method for QKD applications, the LDC has a high-speed slew rate while simplifying the dc bias module.

For the decoy-state BB84 protocol, in order to drive the electro-optic modulator to prepare the required intensity states or polarization states, the MDC should be able to supply three or four voltages with required amplitudes. The structure of the self-designed modulator driver chip (MDC), which is based on the same 130-nm CMOS process, is illustrated in Fig. 1(c) [59]. The MDC includes three independent channels, each of which is composed of a pulse-generation module, an SDC module, an active feedback amplifier, and a drop-down OD output stage. Among them, the SDC and the pulse-generation-module structure are similar to the above-mentioned LDC. To maintain a good bandwidth during the step-by-step amplification of the drive capability, the interleaved nested active-feedback structure is adopted for the preamplification stage.

The MDC realizes the output of the four-level amplitude signals by gating the three input channels individually. The output amplitude of each channel can be adjusted individually by setting different external analog voltages V_{ref}. On the basis of the input arbitrary one-hot code, one of the three channels is selected and output using the same OD structure. When none of the three channels are triggered, the output is the default zero level. Through precise tuning of the amplitudes of the three channels, the MDC is able to generate the required driving signals for intensity modulation or polarization modulation with one single chip.

III. EXPERIMENTAL SETUP

On the basis of the self-developed integrated photonics and integrated electronics, successful QKD experiments are conducted to demonstrate the feasibility and characterize the performance of our chip-based QKD system. The schematic of the experimental setup is shown in Fig. 2. The four integrated chips (a PIC, a LDC, and two MDCs) are adopted to prepare the required quantum states for the decoy-state BB84 protocol. Micrographs of the PIC, LDC, and MDC are shown in Figs. 2(b)–2(d), respectively.

Alice employs a self-developed pulse generator (PG) board to realize the system control functions. On the

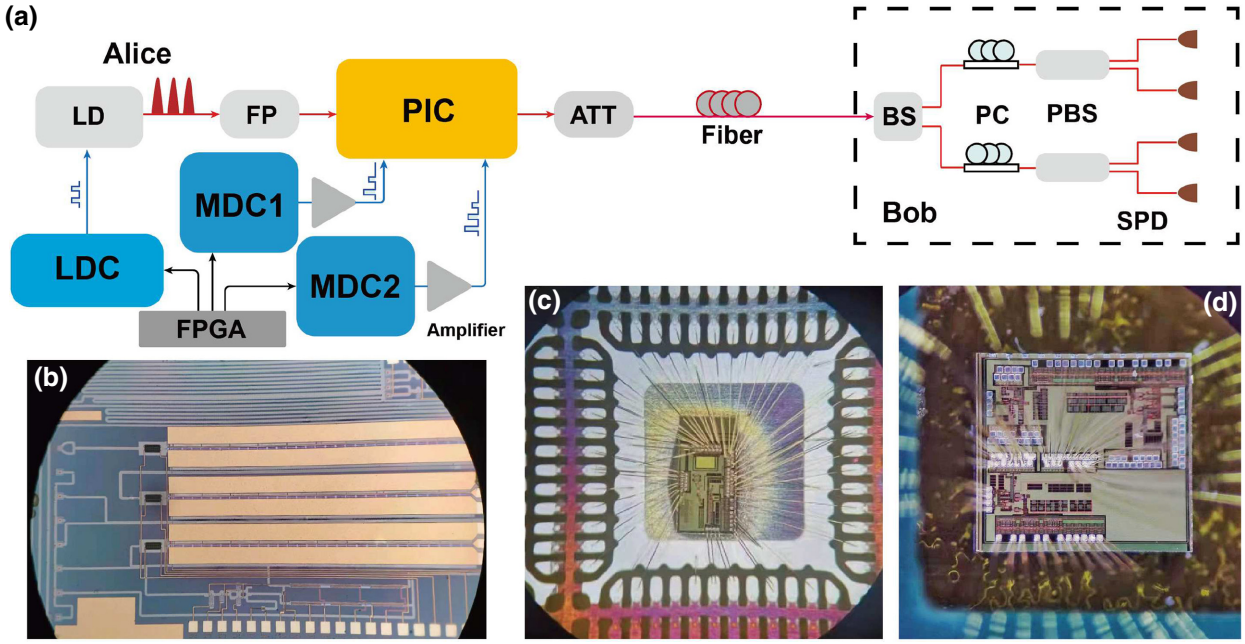


FIG. 2. (a) The experimental setup of the chip-based QKD. (b)–(d) Microscope images of the PIC, LDC, and MDC chip, respectively. LD, laser diode; FP, Fabry-Perot filter; FPGA, field-programmable gate array; ATT, attenuator; BS, beam splitter; PC, polarization controller; PBS, polarizing beam splitter; SPD, single-photon detector.

basis of the prepared physical random numbers, the field-programmable gate array (FPGA) generates multichannel random triggering signals. The LDC, which can generate a pulse current with a maximum amplitude of 60 mA and a variable pulse width ranging from 400 to 1200 ps, drives a 1550-nm LD at a repetition rate of 312.5 MHz to produce phase-randomized periodic optical pulses. The Fabry-Perot (FP) etalon filter is used for narrow-line-width spectral filtering. On the basis of the random triggering signals, two MDCs (MDC1 and MDC2) are adopted to generate the required driving signals for intensity modulation or polarization modulation for the PIC. Because the maximum signal output amplitudes of the MDC are insufficient, additional amplifiers are added to amplify the driving signals to about 6 V to meet the modulation-voltage requirements of the PIC. Additionally, the temperatures of the LD, the FP filter, and the PIC are stably controlled by thermoelectric controllers to ensure performance stability. The attenuator (ATT) is used to attenuate the prepared quantum states to the single-photon level.

The channel is either a fiber pool or is emulated using a variable optical attenuator (VOA). After that, Bob decodes the polarization states using a module composed of a beam splitter (BS), two polarization controllers (PCs), and two polarizing beam splitters (PBSs). Four single-photon detectors (SPDs) are adopted to detect quantum photons. In our experiments, the two types of superconducting nanowire single-photon detector (SNSPD) and (In, Ga)As avalanche photon diode (APD) are both tested to verify the best performance and practical applications of the integrated chips. The SNSPD works at an ultralow temperature of 2.4 K and has a detection efficiency of approximately 36% and a dark-count rate of approximately 10 counts/s per channel. In comparison, the (In, Ga)As APD is free running at a temperature of $-90\,^{\circ}$C and has a detection efficiency of approximately 10% and a dark-count rate of approximately 30 counts/s per channel. The synchronization method using quantum photons [60] is adopted to realize time synchronization between Alice and Bob during data postprocessing.

IV. EXPERIMENTAL RESULTS

We first test the performance of the integrated chips individually and the corresponding results are depicted in Fig. 3. The measured results of the monitor photodetector (MPD) current and the output optical power when scanning the applied continuous dc voltage of the PIC IM are shown in Fig. 3(a). The maximum extinction ratio reaches up to 29.4 dB with a half-wave voltage of 3.27 V. When balancing the incident light of the two arms and scanning the applied voltages of the PIC PM2, the four polarization states of two mutually unbiased bases for the BB84 protocol can be prepared, as shown in Fig. 3(b). The angles between two orthogonal polarization states are 176.6° and 172.6°, which yields a static polarization extinction ratio (PER) of 36.5 dB and 29.8 dB, respectively. Due to the unitary transformation introduced by the single-mode fiber

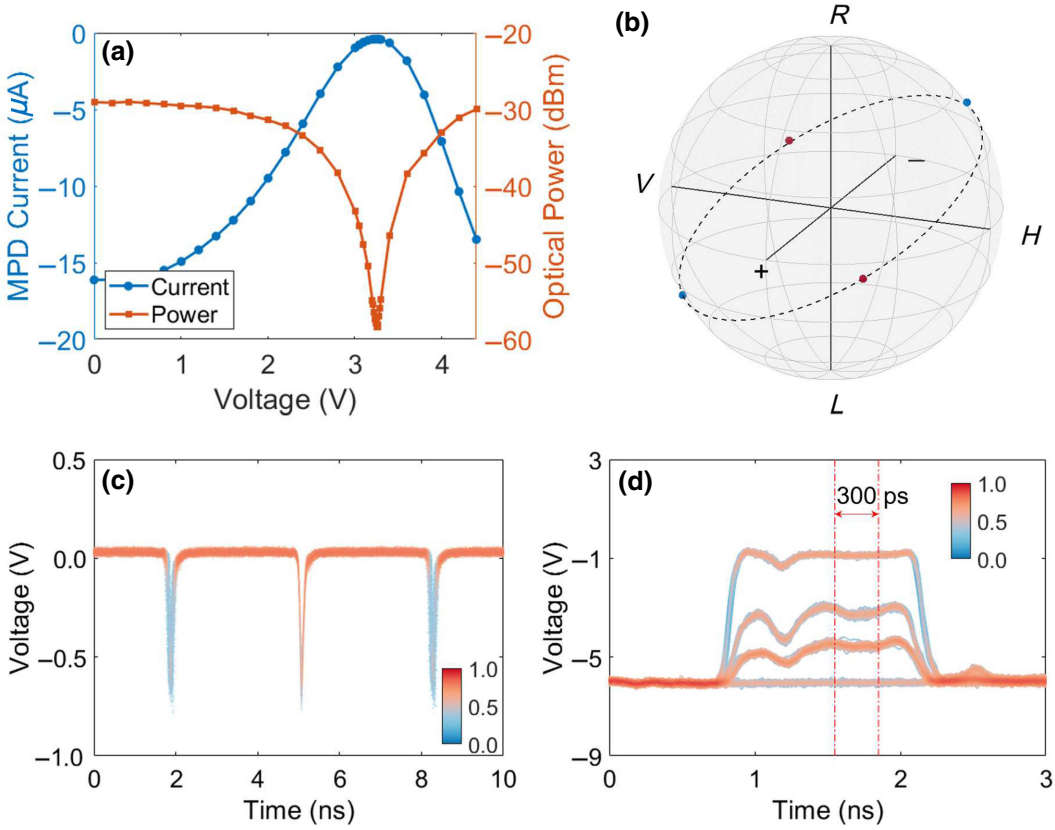


FIG. 3. (a) The measured results of the MPD current (blue dots) and the output optical power (orange squares) when scanning the applied continuous dc voltage of the PIC IM. (b) The four prepared polarization states for the BB84 protocol on the Poincaré sphere. (c) The measured short optical pulses using a 12-GHz-bandwidth photoreceiver. (d) The amplified MDC output signals, which have four independent random amplitudes. The data in (c) and (d) are acquired by a 16-GHz-bandwidth oscilloscope and the color bar represents the normalized frequency of occurrence.

(SMF) output of the PIC, the measured polarization states have an overall rotation on the Poincaré sphere compared to the theoretical polarization states. This can be simply compensated using a PC and does not affect the application of the PIC.

A 12-GHz-bandwidth photoreceiver (Newport, model 1544-B) and a 16-GHz-bandwidth oscilloscope (DSA-X 91604A) are used to measure the generated short optical pulses and amplified MDC output signals and the corresponding results are shown in Figs. 3(c) and 3(d), respectively. The measured full width at half maximum (FWHM) of the optical pulses is approximately 34 ps.

The measured amplified MDC output signals have a maximum amplitude of approximately 6 V and a root-mean-square (rms) value of less than 98 mV within the 300-ps period marked in Fig. 3(d), which is sufficient to drive the PIC to prepare the required quantum states. Note that there is some reflection in the first half of the signals, caused by impedance mismatch within the chip. The second half is a perfect plateau lasting for about 400 ps, which can be precisely adjusted to match the incident short optical pulses and realize stable state modulation of the PIC.

On the basis of a 28-dB emulated channel loss, the measured polarization error rate under random modulation is approximately 0.41% within 3 h [as shown in Fig. 4(a)], which yields a PER in excess of 23.7 dB. This PER under random modulation is lower than that of above-mentioned static PER, this being mainly attributed to the amplitude deviation of the amplified MDC output signals.

We adopt the decoy-state theory to extract the secure keys [31] and the key-generation rate R is given as follows:

$$R \geq 0.5\{-Q_\mu f\,(E_\mu)H_2(E_\mu) + Q_1[1 - H_2(e_1)]\}, \qquad (1)$$

where Q_μ and E_μ are the gain and QBER of the signal state, Q_1 and e_1 are the gain and QBER of the single-photon state, f is the error correction function, and H_2 is the binary Shannon entropy. In the finite-key scenario, the failure probability is set to 10^{-10} for the statistical fluctuation [61]. On the basis of the self-developed integrated photonics and integrated electronics, a series of QKD experiments is performed with the emulated channel using either a fiber pool or a VOA and with the two

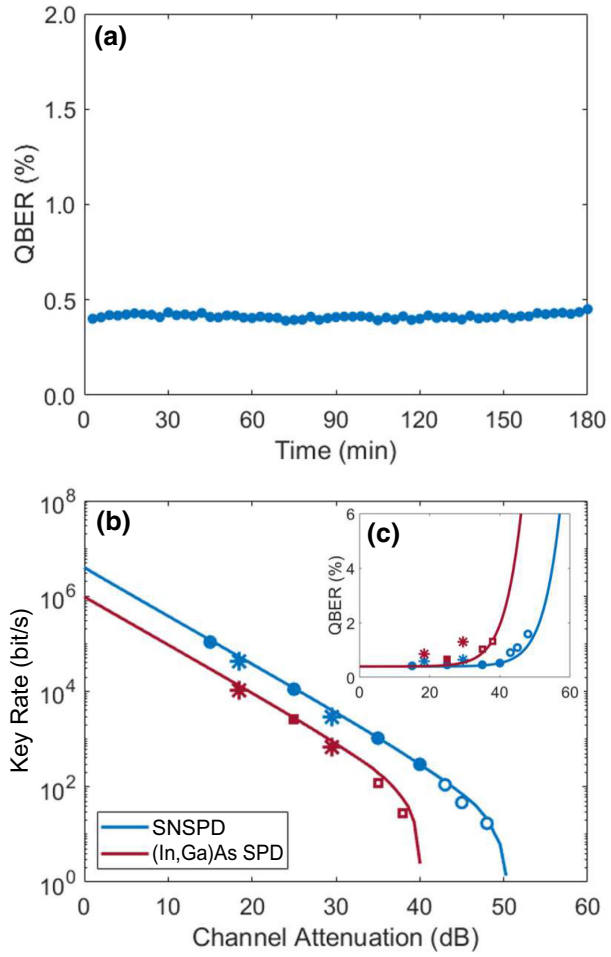


FIG. 4. (a) The measured polarization error rate under random modulation. The channel is emulated using a 28-dB VOA and the measured polarization error rate is approximately 0.41% ± 0.06% within 3 h. All data are collected without any active adjustment of the chip-based QKD system. (b),(c) The extracted quantum bit error rate (QBER) and secure key rate (SKR) with the emulated channels using either a fiber pool or a VOA and with the two types of SNSPDs and (In, Ga)As APDs. The blue and red lines represent the theoretically calculated SKR and QBER with the SNSPD and the (In, Ga)As SPD, respectively. The solid circles and squares are measurement results of emulated losses using the VOA with quantum photon synchronization, while the hollow circles and squares are measurement results with local synchronization. The asterisks are the measurement results for the 100-km and 150-km fiber spools, respectively.

types of SNSPDs and (In, Ga)As APDs. The average photon numbers of the signal, decoy, and vacuum states are set to 0.8, 0.1, and 0.0016, with probabilities of 1/2, 1/4, and 1/4, respectively.

The extracted QBER and secure key rate (SKR) are illustrated in Figs. 4(b) and 4(c). For the QKD experiments, the secure keys are extracted by an accumulation of 10 min (or a total photon number of 10×10^6) for each data point. As the maximum click rates of our SNSPD and APD are about 2×10^6 counts/s and 20×10^3 counts/s for each channel, there are no experimental data with a channel loss lower than 15 dB due to detector saturation. For a channel loss over 43 dB with the SNSPD and 35 dB with the (In, Ga)As APD, the total count rate of the quantum photons is too low to recover the synchronization signal. Hence an extra local synchronization signal is used. On the basis of the SNSPD, SKRs of 108.7 kbit/s and 17 bit/s are obtained with 15-dB and 48-dB emulated channel losses. These measurement results fit well with the theoretical results and the maximum channel loss that can generate positive keys is over 50 dB. Next, we replace the optical VOA with commercial fiber spools. The obtained SKRs are 42.7 kbit/s and 2.9 kbit/s for the 100-km and 150-km fiber spools, respectively, and the corresponding QBERs are 0.59% and 0.64%. Working toward practical applications of the integrated chips, we conduct similar QKD experiments using the (In, Ga)As APD. Due to the lower detection efficiency, the obtained SKRs are 10.5 kbps and 667.1 bps for the 100-km and 150-km fiber spools, respectively. The maximum channel loss that can generate positive keys is approximately 40 dB, which corresponds to the attenuation of 200-km standard fiber (approximately 0.2 dB/km).

V. DISCUSSION AND CONCLUSIONS

In summary, we present a prototype of an integrated optoelectronic QKD transmitter by developing the technologies of integrated silicon photonics and electronics and we demonstrate successful QKD experiments at a repetition frequency of 312.5 MHz using standard fiber and emulated channel loss. The PIC integrates the essential encoding components for the decoy-state BB84 protocol using polarization encoding, while the two electronic chips are able to drive the LD to generate short optical pulses and drive the electro-optic modulator to prepare the required quantum states. For the 100-km fiber spool and 40-dB emulated loss, the obtained SKRs in the finite-key scenario are 42.7 kbps and 295.5 bps, respectively. Compared with QKD systems consisting of discrete optical and electronic devices, the adoption of integrated photonics and electronics has the potential to improve system performance, integration, stability, and scalability and reduce the cost significantly. Our work hopefully takes a fundamental step toward the ultimate solution for the next generation of a system on a chip or a system in a package.

The performance of PICs may differ within chips due to process deviation. In our experiment, a PIC with good overall performance is chosen, i.e., a lower half-wave voltage to meet the driving capability of our electronic chips and appropriate extinction ratios to support better QKD performance. Follow-up works could focus on several aspects. First, the influence of the amplitude fluctuation

of the driving signals on the prepared polarization states should be further analyzed. Second, the first half of the pulse driving signal provided by the MDC suffers from vibration due to imperfect impedance matching, which limits the system repetition frequency. By optimizing the design, layout, fabricating, and packaging process of the electronic chips, the working frequency of these chips can be increased to several gigahertz. Third, attempts can be made to package the electronic chips and the amplifiers in the same chip, which can improve the signal integrity and at the same time improve the integration and reliability of the chip. For photonic devices, integrated lasers are realized by the molecular bonding of III-V heterostructures on silicon [62]. Then, it is possible to try to integrate the silicon PIC and the hybrid III-V silicon-laser chip on the same substrate. Finally, attempts can be made to copackage the integrated photonics and electronics devices to realize the ultimate system-in-a-package solution. Additionally, the application of integrated photonics and electronics in some scenarios with limited size and weight, such as unmanned-aerial-vehicle- and satellite-based QKD, can be explored simultaneously. Chip-based QKD experiments with other protocols such as differential phase shifting (DPS) [63] and differential phase-time shifting (DPTS) [64] can also be attempted in the follow-up research.

ACKNOWLEDGMENTS

This work is supported by the National Key Research and Development Program of China (Grants No. 2020YFA0309701, No. 2020YFA0309703, and No. 2020YFE0200600); the Shanghai Municipal Science and Technology Major Project (Grant No. 2019SHZDZX01); and the Anhui Provincial Natural Science Foundation (Grants No. 2008085MA29 and No. 2008085J03). We would like to thank the electronic design automation (EDA) center of the Chinese Academy of Sciences for supporting the application specific integrated circuit (ASIC) tapeout and Quancore Technology Co., Ltd. for the realization of the PIC. C.-X.Z. and Z.-Y.C. contributed equally to this work.

[1] C. H. Bennett and G. Brassard, in *Proceedings of IEEE International Conference on Computers, Systems, and Signal Processing* (India, 1984), p. 175.

[2] A. Muller, J. Breguet, and N. Gisin, Experimental demonstration of quantum cryptography using polarized photons in optical fibre over more than 1 km, Europhys. Lett. **23**, 383 (1993).

[3] C. Z. Peng, J. Zhang, D. Yang, W. B. Gao, H. X. Ma, H. Yin, H. P. Zeng, T. Yang, X. B. Wang, and J. W. Pan, Experimental Long-Distance Decoy-State Quantum Key Distribution Based on Polarization Encoding, Phys. Rev. Lett. **98**, 010505 (2007).

[4] D. Rosenberg, J. W. Harrington, P. R. Rice, P. A. Hiskett, C. G. Peterson, R. J. Hughes, A. E. Lita, S. W. Nam, and J. E. Nordholt, Long-Distance Decoy-State Quantum Key Distribution in Optical Fiber, Phys. Rev. Lett. **98**, 010503 (2007).

[5] H. L. Yin, T. Y. Chen, Z. W. Yu, H. Liu, L. X. You, Y. H. Zhou, S. J. Chen, Y. Mao, M. Q. Huang, W. J. Zhang, H. Chen, M. J. Li, D. Nolan, F. Zhou, X. Jiang, Z. Wang, Q. Zhang, X. B. Wang, and J. W. Pan, Measurement-Device-Independent Quantum Key Distribution over a 404 km Optical Fiber, Phys. Rev. Lett. **117**, 190501 (2016).

[6] A. Boaron, G. Boso, D. Rusca, C. Vulliez, C. Autebert, M. Caloz, M. Perrenoud, G. Gras, F. Bussières, M.-J. Li, D. Nolan, A. Martin, and H. Zbinden, Secure Quantum Key Distribution over 421 km of Optical Fiber, Phys. Rev. Lett. **121**, 190502 (2018).

[7] J. P. Chen, C. Zhang, Y. Liu, C. Jiang, W. J. Zhang, Z. Y. Han, S. Z. Ma, X. L. Hu, Y. H. Li, H. Liu, F. Zhou, H. F. Jiang, T. Y. Chen, H. Li, L. X. You, Z. Wang, X. B. Wang, Q. Zhang, and J. W. Pan, Twin-field quantum key distribution over a 511 km optical fibre linking two distant metropolitan areas, Nat. Photon. **15**, 570 (2021).

[8] M. Pittaluga, M. Minder, M. Lucamarini, M. Sanzaro, R. I. Woodward, M. J. Li, Z. Yuan, and A. J. Shields, 600-km repeater-like quantum communications with dual-band stabilization, Nat. Photon. **15**, 530 (2021).

[9] C. H. Bennett, F. Bessette, G. Brassard, L. Salvail, and J. Smolin, Experimental quantum cryptography, J. Crypt. **5**, 3 (1992).

[10] T. Schmitt-Manderbach, H. Weier, M. Fürst, R. Ursin, F. Tiefenbacher, T. Scheidl, J. Perdigues, Z. Sodnik, C. Kurtsiefer, J. G. Rarity, A. Zeilinger, and H. Weinfurter, Experimental Demonstration of Free-Space Decoy-State Quantum Key Distribution over 144 km, Phys. Rev. Lett. **98**, 010504 (2007).

[11] J. Y. Wang, *et al.*, Direct and full-scale experimental verifications towards ground-satellite quantum key distribution, Nat. Photon. **7**, 387 (2013).

[12] S. Nauerth, F. Moll, M. Rau, C. Fuchs, J. Horwath, S. Frick, and H. Weinfurter, Air-to-ground quantum communication, Nat. Photon. **7**, 382 (2013).

[13] S. K. Liao, *et al.*, Long-distance free-space quantum key distribution in daylight towards inter-satellite communication, Nat. Photon. **11**, 509 (2017).

[14] Y. Cao, *et al.*, Long-Distance Free-Space Measurement-Device-Independent Quantum Key Distribution, Phys. Rev. Lett. **125**, 260503 (2020).

[15] S. K. Liao, *et al.*, Satellite-to-ground quantum key distribution, Nature **549**, 43 (2017).

[16] J. Yin, *et al.*, Satellite-based entanglement distribution over 1200 km, Science **356**, 1140 (2017).

[17] J. Yin, *et al.*, Satellite-to-Ground Entanglement-Based Quantum Key Distribution, Phys. Rev. Lett. **119**, 200501 (2017).

[18] S. K. Liao, *et al.*, Satellite-Relayed Intercontinental Quantum Network, Phys. Rev. Lett. **120**, 030501 (2018).

[19] Y. A. Chen, *et al.*, An integrated space-to-ground quantum communication network over 4,600 km, Nature **589**, 214 (2021).

[20] C. Elliott, A. Colvin, D. Pearson, O. Pikalo, J. Schlafer, and H. Yeh, Current status of the DARPA quantum network, Quantum Inf. Comput. III **5815**, 138 (2005).

[21] M. Peev, *et al.*, The SECOQC quantum key distribution network in Vienna, New J. Phys. **11**, 075001 (2009).
[22] M. Sasaki, *et al.*, Field test of quantum key distribution in the Tokyo QKD Network, Opt. Express **19**, 10387 (2011).
[23] D. Stucki, *et al.*, Long-term performance of the SwissQuantum quantum key distribution network in a field environment, New J. Phys. **13**, 123001 (2011).
[24] S. Wang, *et al.*, Field and long-term demonstration of a wide area quantum key distribution network, Opt. Express **22**, 21739 (2014).
[25] J. F. Dynes, A. Wonfor, W. W. Tam, A. W. Sharpe, R. Takahashi, M. Lucamarini, A. Plews, Z. L. Yuan, A. R. Dixon, J. Cho, Y. Tanizawa, J. P. Elbers, H. Greißer, I. H. White, R. V. Penty, and A. J. Shields, Cambridge quantum network, npj Quantum Inf. **5**, 101 (2019).
[26] T. Y. Chen, *et al.*, Implementation of a 46-node quantum metropolitan area network, npj Quantum Inf. **7**, 134 (2021).
[27] V. Scarani, H. Bechmann-Pasquinucci, N. J. Cerf, M. Dušek, N. Lütkenhaus, and M. Peev, The security of practical quantum key distribution, Rev. Mod. Phys. **81**, 1301 (2009).
[28] F. Xu, X. Ma, Q. Zhang, H.-K. Lo, and J.-W. Pan, Secure quantum key distribution with realistic devices, Rev. Mod. Phys. **92**, 025002 (2020).
[29] S. Sajeed, P. Chaiwongkhot, A. Huang, H. Qin, V. Egorov, A. Kozubov, A. Gaidash, V. Chistiakov, A. Vasiliev, A. Gleim, and V. Makarov, An approach for security evaluation and certification of a complete quantum communication system, Sci. Rep. **11**, 1 (2021).
[30] X. B. Wang, Beating the Photon-Number-Splitting Attack in Practical Quantum Cryptography, Phys. Rev. Lett. **94**, 230503 (2005).
[31] H. K. Lo, X. Ma, and K. Chen, Decoy State Quantum Key Distribution, Phys. Rev. Lett. **94**, 230504 (2005).
[32] H. K. Lo, M. Curty, and B. Qi, Measurement-Device-Independent Quantum Key Distribution, Phys. Rev. Lett. **108**, 130503 (2012).
[33] M. Lucamarini, Z. L. Yuan, J. F. Dynes, and A. J. Shields, Overcoming the rate-distance barrier of quantum key distribution without using quantum repeaters, Nature **557**, 400 (2018).
[34] G. L. Roberts, M. Pittaluga, M. Minder, M. Lucamarini, J. F. Dynes, Z. L. Yuan, and A. J. Shields, Patterning-effect mitigating intensity modulator for secure decoy-state quantum key distribution, Opt. Lett. **43**, 5110 (2018).
[35] Y. Li, Y.-H. Li, H.-B. Xie, Z.-P. Li, X. Jiang, W.-Q. Cai, J.-G. Ren, J. Yin, S.-K. Liao, and C.-Z. Peng, High-speed robust polarization modulation for quantum key distribution, Opt. Lett. **44**, 5262 (2019).
[36] X. Zhong, J. Hu, M. Curty, L. Qian, and H. K. Lo, Proof-of-Principle Experimental Demonstration of Twin-Field Type Quantum Key Distribution, Phys. Rev. Lett. **123**, 100506 (2019).
[37] E. Miller, Integrated optics: An introduction, The Bell Syst. Tech. J. **48**, 2059 (1969).
[38] C. Ma, W. D. Sacher, Z. Tang, J. C. Mikkelsen, Y. Yang, F. Xu, T. Thiessen, H.-K. Lo, and J. K. S. Poon, Silicon photonic transmitter for polarization-encoded quantum key distribution, Optica **3**, 1274 (2016).
[39] J. E. Kennard, P. Sibson, S. Stanisic, C. Erven, J. L. O'Brien, and M. G. Thompson, Integrated silicon photonics for high-speed quantum key distribution, Optica **4**, 172 (2017).
[40] P. Sibson, C. Erven, M. Godfrey, S. Miki, T. Yamashita, M. Fujiwara, M. Sasaki, H. Terai, M. G. Tanner, C. M. Natarajan, R. H. Hadfield, J. L. O'Brien, and M. G. Thompson, Chip-based quantum key distribution, Nat. Commun. **8**, 13984 (2017).
[41] T. K. Paraïso, T. Roger, D. G. Marangon, I. De Marco, M. Sanzaro, R. I. Woodward, J. F. Dynes, Z. Yuan, and A. J. Shields, A photonic integrated quantum secure communication system, Nat. Photon. **15**, 850 (2021).
[42] T. K. Paraïso, I. De Marco, T. Roger, D. G. Marangon, J. F. Dynes, M. Lucamarini, Z. Yuan, and A. J. Shields, A modulator-free quantum key distribution transmitter chip, npj Quantum Inf. **5**, 42 (2019).
[43] K. Wei, W. Li, H. Tan, Y. Li, H. Min, W.-J. Zhang, H. Li, L. You, Z. Wang, X. Jiang, T.-Y. Chen, S.-K. Liao, C.-Z. Peng, F. Xu, and J.-W. Pan, High-speed measurement-device-independent quantum key distribution with integrated silicon photonics, Phys. Rev. X **10**, 031030 (2020).
[44] H. Semenenko, P. Sibson, A. Hart, M. G. Thompson, J. G. Rarity, and C. Erven, Chip-based measurement-device-independent quantum key distribution, Optica **7**, 238 (2020).
[45] G. Zhang, J. Y. Haw, H. Cai, F. Xu, S. M. Assad, J. F. Fitzsimons, X. Zhou, Y. Zhang, S. Yu, J. Wu, W. Ser, L. C. Kwek, and A. Q. Liu, An integrated silicon photonic chip platform for continuous-variable quantum key distribution, Nat. Photon. **13**, 839 (2019).
[46] C. Wang, M. Zhang, X. Chen, M. Bertrand, A. Shams-Ansari, S. Chandrasekhar, P. Winzer, and M. Lončar, Integrated lithium niobate electro-optic modulators operating at CMOS-compatible voltages, Nature **562**, 101 (2018).
[47] D. Bunandar, A. Lentine, C. Lee, H. Cai, C. M. Long, N. Boynton, N. Martinez, C. DeRose, C. Chen, M. Grein, D. Trotter, A. Starbuck, A. Pomerene, S. Hamilton, F. N. C. Wong, R. Camacho, P. Davids, J. Urayama, and D. Englund, Metropolitan quantum key distribution with silicon photonics, Phys. Rev. X **8**, 021009 (2018).
[48] M. Avesani, L. Calderaro, M. Schiavon, A. Stanco, C. Agnesi, A. Santamato, M. Zahidy, A. Scriminich, G. Foletto, G. Contestabile, M. Chiesa, D. Rotta, M. Artiglia, A. Montanaro, M. Romagnoli, V. Sorianello, F. Vedovato, G. Vallone, and P. Villoresi, Full daylight quantum-key-distribution at 1550 nm enabled by integrated silicon photonics, npj Quantum Inf. **7**, 93 (2021).
[49] H. Ransijn, G. Salvador, D. D. Daugherty, and K. D. Gaynor, A 10-Gb/s laser/modulator driver IC with a dual-mode actively matched output buffer, IEEE J. Solid-State Circuits **36**, 1314 (2001).
[50] C. Knochenhauer, J. C. Scheytt, and F. Ellinger, A compact, low-power 40-GBit/s modulator driver with 6-V differential output swing in 0.25-μm SiGe BiCMOS, IEEE J. Solid-State Circuits **46**, 1137 (2011).

[51] X. Wang, F. Liang, B. Feng, C. Zhu, Y. Zhu, and G. Jin, Integrated electronics in 130 nm CMOS process for quantum key distribution sender device, Rev. Sci. Instrum. **91**, 034701 (2020).

[52] W. Jiang, R. Scott, and M. J. Deen, Differential quench and reset circuit for single-photon avalanche diodes, J. Lightwave Technol. **39**, 7334 (2021).

[53] A. H. Atabaki, S. Moazeni, F. Pavanello, H. Gevorgyan, J. Notaros, L. Alloatti, M. T. Wade, C. Sun, S. A. Kruger, H. Meng, K. Al Qubaisi, I. Wang, B. Zhang, A. Khilo, C. V. Baiocco, M. A. Popović, V. M. Stojanović, and R. J. Ram, Integrating photonics with silicon nanoelectronics for the next generation of systems on a chip, Nature **556**, 349 (2018).

[54] C. Huang, S. Fujisawa, T. F. de Lima, A. N. Tait, E. C. Blow, Y. Tian, S. Bilodeau, A. Jha, F. Yaman, H. T. Peng, H. G. Batshon, B. J. Shastri, Y. Inada, T. Wang, and P. R. Prucnal, A silicon photonic-electronic neural network for fibre nonlinearity compensation, Nat. Electron. **4**, 837 (2021).

[55] X. Zheng, P. Zhang, R. Ge, L. Lu, G. He, Q. Chen, F. Qu, L. Zhang, X. Cai, Y. Lu, S. Zhu, P. Wu, and X.-S. Ma, Heterogeneously integrated, superconducting silicon-photonic platform for measurement-device-independent quantum key distribution, Adv. Photon. **3**, 1 (2021).

[56] C. Bruynsteen, M. Vanhoecke, J. Bauwelinck, and X. Yin, Integrated balanced homodyne photonic-electronic detector for beyond 20 GHz shot-noise-limited measurements, Optica **8**, 1146 (2021).

[57] F. Beutel, H. Gehring, M. A. Wolff, C. Schuck, and W. Pernice, Detector-integrated on-chip QKD receiver for GHz clock rates, npj Quantum Inf. **7**, 40 (2021).

[58] B. Feng, F. Liang, X. Wang, C. Zhu, Y. Zhu, and G. Jin, A laser source driver with adjustable amplitude and pulse-width in 130-nm CMOS technology for quantum key distribution experiments, Rev. Sci. Instrum. **90**, 1 (2019).

[59] C. Zhu, F. Liang, B. Feng, X. Wang, Y. Zhu, and C. Peng, in *Proceedings of International Conference on ASIC* (2019), p. 1.

[60] C.-Z. Wang, Y. Li, W.-Q. Cai, W.-Y. Liu, S.-K. Liao, and C.-Z. Peng, Synchronization using quantum photons for satellite-to-ground quantum key distribution, Opt. Express **29**, 29595 (2021).

[61] Z. Zhang, Q. Zhao, M. Razavi, and X. Ma, Improved key-rate bounds for practical decoy-state quantum-key-distribution systems, Phys. Rev. A **95**, 012333 (2017).

[62] C. Agnesi, M. Avesani, A. Stanco, P. Villoresi, and G. Vallone, All-fiber self-compensating polarization encoder for quantum key distribution, Opt. Lett. **44**, 2398 (2019).

[63] K. Inoue, E. Waks, and Y. Yamamoto, Differential Phase Shift Quantum Key Distribution, Phys. Rev. Lett. **89**, 037902 (2002).

[64] D. Bacco, J. B. Christensen, M. A. Castaneda, Y. Ding, S. Forchhammer, K. Rottwitt, and L. K. Oxenløwe, Two-dimensional distributed-phase-reference protocol for quantum key distribution, Sci. Rep. **6**, 1 (2016).